



Article

Cyano-Bridged Dy(III) and Ho(III) Complexes with Square-Wave Structure of the Chains

Valentina D. Sasnovskaya¹, Leokadiya V. Zorina^{2,*}, Sergey V. Simonov², Artem D. Talantsev¹ and Eduard B. Yagubskii^{1,*}

¹ Institute of Problems of Chemical Physics RAS, 142432 Chernogolovka, Russia; sasnovskayavd@rambler.ru (V.D.S.); artgtx32@mail.ru (A.D.T.)

² Institute of Solid State Physics RAS, 142432 Chernogolovka, Russia; simonov@issp.ac.ru

* Correspondence: zorina@issp.ac.ru (L.V.Z.); yagubski@gmail.com (E.B.Y.)

Abstract: Four new cyano-bridged $\text{Dy}^{\text{III}}\text{-Cr}^{\text{III}}$, $\text{Dy}^{\text{III}}\text{-Fe}^{\text{III}}$, $\text{Ho}^{\text{III}}\text{-Cr}^{\text{III}}$ and $\text{Ho}^{\text{III}}\text{-Fe}^{\text{III}}$ bimetallic coordination polymers were synthesized by the reaction of $[\text{Ln}(\text{H}_2\text{dapsc})(\text{H}_2\text{O})_4](\text{NO}_3)_3$ ($\text{Ln} = \text{Dy}, \text{Ho}$); $\text{H}_2\text{dapsc} = 2,6\text{-diacetylpyridinebis(semicarbazone)}$ with $\text{K}_3[\text{M}(\text{CN})_6]$ ($\text{M} = \text{Cr}, \text{Fe}$) in H_2O , resulting in the substitution of two water molecules in the coordination sphere of rare earth by paramagnetic tricharged hexacyanides of Fe and Cr. The complexes are isostructural and consist of alternating $[\text{Ln}(\text{H}_2\text{dapsc})(\text{H}_2\text{O})_2]^{3+}$ and $[\text{M}(\text{CN})_6]^{3-}$ units linked by bridges of two *cis*-cyano ligands of the anion to form square-wave chains. The ac magnetic measurements revealed that the DyCr and DyFe complexes are field-induced single molecule magnets, while their Ho analogs do not exhibit slow magnetic relaxation.

Keywords: field-induced single-molecular magnets; nine-coordinate complexes; $\text{Ln}(\text{III})$ complexes; H_2dapsc ligand; crystal structure; dc and ac magnetic properties



Citation: Sasnovskaya, V.D.; Zorina, L.V.; Simonov, S.V.; Talantsev, A.D.; Yagubskii, E.B. Cyano-Bridged Dy(III) and Ho(III) Complexes with Square-Wave Structure of the Chains. *Inorganics* **2022**, *10*, 41. <https://doi.org/10.3390/inorganics10040041>

Academic Editor: Akseli Mansikkamäki

Received: 9 March 2022

Accepted: 27 March 2022

Published: 29 March 2022

Publisher's Note: MDPI stays neutral with regard to jurisdictional claims in published maps and institutional affiliations.



Copyright: © 2022 by the authors. Licensee MDPI, Basel, Switzerland. This article is an open access article distributed under the terms and conditions of the Creative Commons Attribution (CC BY) license (<https://creativecommons.org/licenses/by/4.0/>).

1. Introduction

Molecular nanomagnets—SMMs (single-molecule magnets), SIMs (single-ion magnets) and SCMs (single-chain magnets)—are intensively studied owing to their unique properties such as superparamagnetism, magnetic bi-stability, slow magnetic relaxation, blocking and quantum tunneling of magnetization as well as potential application as components of high-density information storages, spintronic and quantum computing devices [1]. Among them the lanthanide-based SIMs attract a special attention because of strong uniaxial magnetic anisotropy of the lanthanide ions (especially 4f-lanthanides Tb^{3+} , Dy^{3+} , Ho^{3+} , Er^{3+}) caused by enhanced spin-orbital coupling, which can improve the characteristics of molecular nanomagnets by increasing the values of spin reversal barrier, U_{eff} , and blocking temperature of magnetization, T_B [2,3]. In addition, the geometry of the ligand environment also plays a critical role, since it can enhance the local magnetic anisotropy [4,5]. In the case of rare-earth ions, the spatial distribution of the electrons in the different 4f orbitals leads to inherent anisotropic shapes of electronic density: oblate (Tb , Ho , Dy) and prolate (Er , Tm , Yb), equatorially or axially elongated f-electron charge clouds, respectively. Based on the 4f electron density shape of the rare earths, Rinehard and Long concluded that the oblate shape of the lanthanide ion must be stabilized by an axial ligand field, while the prolate shape requires an equatorial ligand field, because such the ligand fields lead to a decrease of electrostatic repulsion between the ligands and metal center and increase the molecular magnetic anisotropy [6]. With this in mind, several seven-coordinate pentagonal-bipyramidal Dy complexes with high U_{eff} and T_B , up to 1800 K and 22 K, respectively, have recently been synthesized [7–12]. These complexes contain weak donor ligands in the equatorial plane, in particular, five molecules of water or pyridine, and strong bulky ligands in the axial positions, such as tricyclohexylphosphine oxide or tert-butoxide.

Our recent efforts to synthesize new lanthanide-based SIMs using the pentadentate N_3O_2 -donor Schiff-base ligand H_2dapsc (2,6-diacetylpyridinebis(semicarbazone), Figure 1), which forms pentagonal-bipyramidal complexes with many 3d metals [13–18], resulted in four isostructural nine-coordination $[\text{Ln}(\text{H}_2\text{dapsc})(\text{H}_2\text{O})_4](\text{NO}_3)_3$ complexes. Two of them with Dy^{3+} and Er^{3+} Kramers ions are field-induced single-ion magnets whereas the Tb^{3+} and Ho^{3+} complexes show absence of slow magnetic relaxation [19]. It should be noted that interaction between adjacent 4f-metals is usually weak because of the core-like character of 4f-electrons shielded by fully filled $5s^2$ and $5p^6$ orbitals. In this reason it is reasonable to construct mixed 4f-3d complexes in order to introduce stronger magnetic coupling along with high magnetic anisotropy of the lanthanide ion. However, magnetic interactions have a dual effect on the SMM properties of 4f ions-based complexes [20]. On the one hand, the weak intramolecular magnetic interaction between the magnetic ions in polynuclear complexes may promote the quantum tunneling of magnetization (QTM) thus accelerating the process of magnetic relaxation [21–25]. On the other hand, strong magnetic exchange coupling can increase the blocking temperature of SMM [26]. The combination of 4f-3d ions can be achieved using hexacyanides of paramagnetic 3d metals $[\text{M}^{\text{III}}(\text{CN})_6]^{3-}$ as a link between 4f ions via cyanide bridges [27]. Recently, by implementing this approach, Tong's group synthesized a trinuclear linear complex $(\text{PPh}_4)[\text{Dy}_2(\text{bbpen})_2\{\text{Fe}(\text{CN})_6\}] \cdot 3.5\text{CH}_3\text{CN}$ that showed a record magnetization barrier of 659 K in d-f SMMs, which made the cyanide-bridged 3d-4f systems more attractive [28].

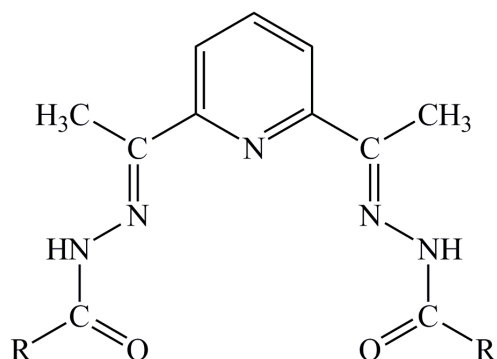


Figure 1. Molecular structure of the pentadentate ligand H_2dapsc ($\text{R} = \text{NH}_2$) and its analog H_2dapbh ($\text{R} = \text{C}_6\text{H}_5$).

We synthesized four new polyheteronuclear cyano-bridged chain compounds on the base of Ln^{III} cationic complexes bearing H_2dapsc ligand ($\text{Ln} = \text{Dy}, \text{Ho}$) and $[\text{M}^{\text{III}}(\text{CN})_6]^{3-}$ anions: $\{[\text{Ln}(\text{H}_2\text{dapsc})(\text{H}_2\text{O})_2][\text{M}(\text{CN})_6]\}_n \cdot 3\text{nH}_2\text{O}$; $\text{Ln}, \text{M} = \text{DyCr}$ (1), DyFe (2), HoCr (3), HoFe (4). Their crystal structures and magnetic properties have been investigated and described in comparison with the initial discrete mononuclear lanthanide complexes.

2. Results and Discussion

2.1. Synthesis

Compounds 1–4 were synthesized by slow diffusion of water solution of $\text{K}_3[\text{M}(\text{CN})_6]$ ($\text{M} = \text{Cr}, \text{Fe}$) through frit with a pore diameter of 10–20 microns into a water or water/ethanol solution of $[\text{Ln}(\text{H}_2\text{dapsc})(\text{H}_2\text{O})_4](\text{NO}_3)_3$ ($\text{Ln} = \text{Dy}, \text{Ho}$), the details are given in the Materials and Methods section. The reaction results in the substitution of two water molecules in the coordination sphere of rare earth by paramagnetic tricharged hexacyanides of Fe or Cr accompanied by formation of infinite chains of alternating $[\text{Ln}(\text{H}_2\text{dapsc})(\text{H}_2\text{O})_2]^{3+}$ cations and $[\text{M}(\text{CN})_6]^{3-}$ anions. Thermogravimetric analysis of the complexes showed the weight loss in the temperature ranges 40–100 °C and 115–170 °C corresponding to the loss of lattice and coordinated water molecules, respectively (Figures S6 and S9 in Supplementary Materials). The decomposition of the complexes starts above 180 K with the release of CN-fragments.

2.2. Description of the Structure

The complexes **1–4** are isostructural and crystallize in the monoclinic $P2_1/c$ space group (Table 1). The asymmetric unit includes one $\{[\text{Ln}(\text{H}_2\text{dapsc})][\text{M}(\text{CN})_6](\text{H}_2\text{O})_2\}$ fragment and three solvent water molecules, all in general positions. An ORTEP drawing of **3** is shown in Figure 2 (the atomic numbering is similar in **1–4**), key bond distances and angles for **1–4** are listed in Table A1 of the Appendix A section.

Table 1. Crystal data and structural refinement parameters for the complexes **1–4**.

	1	2	3	4
Chemical formula	$\text{C}_{17}\text{H}_{25}\text{CrDyN}_{13}\text{O}_7$	$\text{C}_{17}\text{H}_{25}\text{FeDyN}_{13}\text{O}_7$	$\text{C}_{17}\text{H}_{25}\text{CrHoN}_{13}\text{O}_7$	$\text{C}_{17}\text{H}_{25}\text{FeHoN}_{13}\text{O}_7$
Formula weight	738.00	741.85	740.43	744.28
Cell setting	monoclinic	monoclinic	monoclinic	monoclinic
Space group, Z	$P2_1/c$, 4	$P2_1/c$, 4	$P2_1/c$, 4	$P2_1/c$, 4
Temperature (K)	150(1)	150(1)	140(1)	295(1)
a (Å)	12.8451(1)	12.6415(8)	12.8518(7)	12.721(2)
b (Å)	12.7918(1)	12.5812(7)	12.8157(7)	12.661(1)
c (Å)	17.1832(2)	17.0894(13)	17.2114(10)	17.293(2)
α (°)	90	90	90	90
β (°)	103.3953(9)	103.484(6)	103.557(6)	103.040(10)
γ (°)	90	90	90	90
Cell volume (Å ³)	2746.58(4)	2643.1(3)	2755.8(3)	2713.4(6)
ρ (g/cm ³)	1.785	1.864	1.785	1.822
μ , cm ⁻¹	31.56	34.18	33.06	34.91
Refls collected/unique	35374/9358	24896/10290	22589/9216	16823/6386
R_{int}	0.0196	0.0793	0.0306	0.0762
θ_{max} (°)	31.20	28.28	31.00	26.50
Parameters refined	402	403	402	399
Final R_1 , wR_2 [$I > 2\sigma(I)$]	0.0159, 0.0362	0.0496, 0.1157	0.0233, 0.0557	0.0519, 0.0814
Goodness-of-fit	1.006	1.001	1.007	1.000
CCDC number	2156616	2156617	2156618	2156619

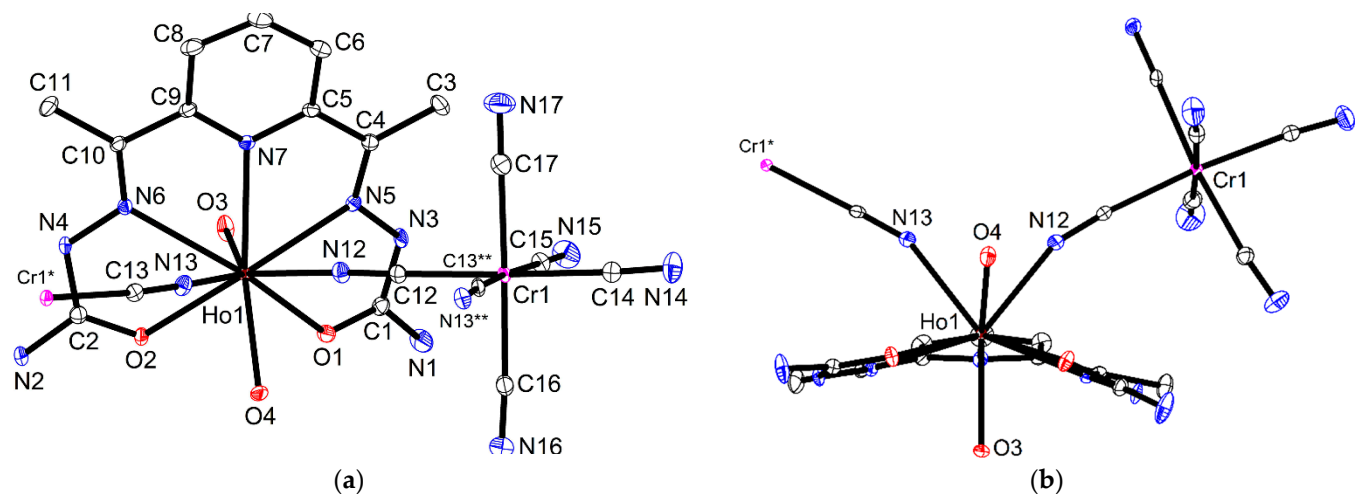


Figure 2. Asymmetric unit in **3** with atom numbering scheme, (a) top and (b) side view, ORTEP drawing with 50% probability ellipsoids). Symmetry codes: * $(1 - x, 0.5 + y, 0.5 - z)$, ** $(1 - x, y - 0.5, 0.5 - z)$.

In the crystal structure of **1–4** cationic $[\text{Ln}^{\text{III}}(\text{H}_2\text{dapsc})(\text{H}_2\text{O})_2]^{3+}$ and anionic $[\text{M}^{\text{III}}(\text{CN})_6]^{3-}$ units are linked through two cyanide bridges in a *cis* mode with respect to M^{3+} ion into neutral 1D chains which have shape of square wave and run along the b -axis (Figure 3a). Within the chain $\text{N}(12)\text{-Ln}(1)\text{-N}(13)$ and $\text{C}(12)\text{-M}(1)\text{-C}(13**)$ angles are 73 and 94°, respectively, when $\text{M} = \text{Cr}$ (in **1** and **3**) and 75 and 95°, respectively, when $\text{M} = \text{Fe}$ (in **2** and **4**, Table A1). The $\text{M}(1)\text{-Ln}(1)\text{-M}(1)$ and $\text{Ln}(1)\text{-M}(1)\text{-Ln}(1)$ angles are 101 and 96°, respectively,

in all the cases. The Ln^{3+} ion is nine-coordinated by three nitrogen and two oxygen atoms of H_2dapsc , two nitrogen atoms from cyanide bridges and two oxygen atoms from aqua ligands. Two $[\text{M}(\text{CN})_6]$ moieties and one coordinated water ($\text{O}(4)$ in Figure 2) are attached to Ln^{3+} ion on the same side of the H_2dapsc ligand while another coordinated water ($\text{O}(3)$) lies on the opposite side of H_2dapsc . As a result, the H_2dapsc ligand is strongly deviated from the planarity (Figure 2, right). The dihedral angle between two semi-carbazone planes defined by 7 non-metallic atoms of two pentagonal cycles from each half of H_2dapsc [$\text{O}(1), \text{C}(1), \text{N}(3), \text{N}(5), \text{C}(4), \text{C}(5), \text{N}(7)$ and $\text{O}(2), \text{C}(2), \text{N}(4), \text{N}(6), \text{C}(10), \text{C}(9), \text{N}(7)$] is $21.52(3), 22.7(2), 22.01(4)$ and $22.22(12)^\circ$ in **1–4**, respectively. For a comparison, in the discrete nine-coordinated mononuclear complexes $[\text{Ln}(\text{H}_2\text{dapsc})(\text{H}_2\text{O})_4](\text{NO}_3)_3$ with $\text{Ln} = \text{Dy}$ and Ho the similar angle is about 13° [19]. Thus, the steric effects are strengthened in **1–4** in the presence of the square-wave chain. According to the shape analysis of these nine-coordinated compounds (Table S1 in Supplementary Materials) the coordination of Dy and Ho in the initial discrete complexes [19] is close to the muffin geometry with a C_s symmetry while distortion parameters in **1–4** is somewhat higher and shape of the polyhedra better fits to the spherical capped square antiprism with a C_{4v} symmetry.

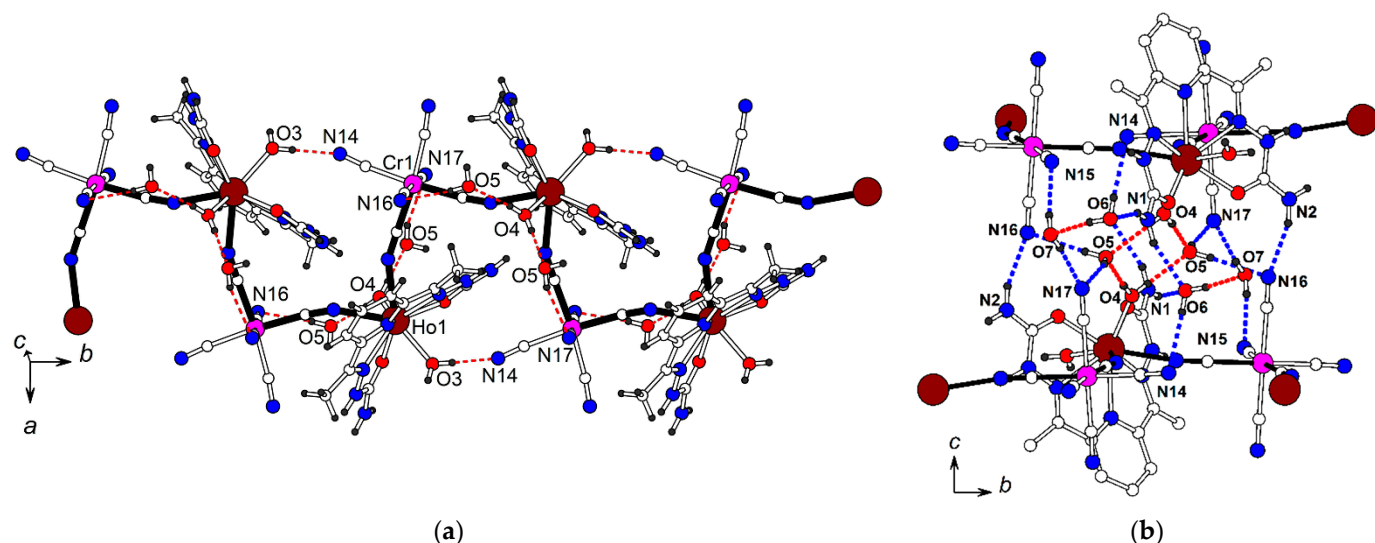


Figure 3. (a) Infinite square-wave chain in **3**. Chain-defining bonds are shown by black solid lines, hydrogen bonds—by red dashed lines. (b) Fragments of two adjacent chains with interchain hydrogen bonding (see Tables S2–S5 for hydrogen bond geometry).

Formation of the square-wave type of chain is supported by strong hydrogen intra-chain bonding shown by red dashed lines in Figure 3a. Details of H-bond geometry is given in Tables S2–S5 and discussed further on the example of structure **3** (HoCr). The shortest hydrogen bond between the adjacent non-connected $[\text{Ho}(\text{H}_2\text{dapsc})(\text{H}_2\text{O})_2]$ and $[\text{Cr}(\text{CN})_6]$ units in the chain, $\text{O}(3)\text{-H}(3\text{wa}) \dots \text{N}(14)$, fixes the square-wave shape. The $\text{H} \dots \text{N}$ distance in this bond is 1.93 \AA , the distance between Ho and Cr ions linked by this hydrogen bond is $7.2368(5) \text{ \AA}$. Second aqua ligand is hydrogen bonded to N atoms of $[\text{Cr}(\text{CN})_6]$ through bridging O(5) water molecules: $\text{O}(4)\text{-H}(4\text{wa}) \dots \text{O}(5)\text{-H}(5\text{wb}) \dots \text{N}(17)$ ($\text{H} \dots \text{O} 1.98 \text{ \AA}, \text{H} \dots \text{N} 2.35 \text{ \AA}$) and $\text{O}(4)\text{-H}(4\text{wb}) \dots \text{O}(5)\text{-H}(5\text{wa}) \dots \text{N}(16)$ ($\text{H} \dots \text{O} 2.08 \text{ \AA}, \text{H} \dots \text{N} 2.25 \text{ \AA}$). The same O(5) water molecule acts as a bridge both in the intrachain and interchain hydrogen bonds (Figure 3b). NH₂-groups of H₂dapsc also participate in hydrogen bonding both inside and between the chains, which are direct or include bridging free water molecules O(6) and O(7) (Figure 3b). $\text{H} \dots \text{O}$ distances in these bonds are $2.00, 2.13 \text{ \AA}$; $\text{H} \dots \text{N}$ ones are $2.11\text{--}2.29 \text{ \AA}$. It should be noted that, unlike to NH₂-groups, the H-bond donor function of NH-groups in H₂dapsc is deactivated, they form only weak hydrogen contacts of $\text{N-H} \dots \text{N}$ type ($\text{H} \dots \text{N}$ of $2.58, 2.64 \text{ \AA}$) to CN-ligands.

Average Fe-C_{CN} distance, $1.94(2) \text{ \AA}$, is about 0.13 \AA shorter than Cr-C_{CN} one, $2.07(1) \text{ \AA}$. Accordingly, the square-wave chain is more compact in **2, 4** than in **1, 3** with intermetallic Ln-

Fe distances a bit shorter than Ln-Cr ones (av. 5.5 Å vs. 5.6 Å, Table A1). The Ln-M distance in the chain between the metals without CN bridge (with hydrogen bond interaction) is 7.2207(2), 7.1216(10), 7.2368(5), 7.1686(10) Å in **1–4**, respectively. The shortest interchain Ln-M distance is 7.4976(2), 7.4179(10), 7.5018(5) and 7.4833(14) Å in **1–4**, respectively. The shortest intrachain and interchain Ln-Ln separations are 8.318 and 8.071 Å in **1**, 8.156 and 7.975 Å in **2**, 8.328 and 8.081 Å in **3**, 8.201 and 8.098 Å in **4**, respectively.

The similar 1D square-wave chains were found in the cationic Ln complexes with water and dimethylformamide (DMF) ligands combined with $[M^{III}(CN)_6]^{3-}$ anions. They are isostructural to each other and have general formula $\{Ln(DMF)_4(H_2O)_2][M(CN)_6\}_n \cdot nH_2O$ ($Ln = Sm, Gd, Tb; M = Cr$ or Fe) [29–32]. Unlike to nine-coordinated complexes in **1–4**, the Ln^{3+} ion in these compounds is eight-coordinated by four oxygen atoms from four DMF ligands, two oxygen atoms from coordinated water molecules and two nitrogen atoms from cyanide bridges. Ln^{3+} and M^{3+} ions are connected into infinite square-wave chain through two cyanide bridges in the *cis* geometry with respect to M^{3+} ion. The chains are further extended into three-dimensional networks through hydrogen bonding interactions [32]. The study of magnetic properties showed that none of these complexes is a SMM. However, the Sm-Fe and Tb-Cr complexes demonstrate a three-dimensional ferromagnetic ordering with $T_c = 3.4$ and ~ 5 K, respectively [30,32].

The H₂dapsc ligand and its analogs are remarkable for the synthesis of new magnetic materials due to their ability to produce metal complexes with pentagonal-bipyramidal (PBP) environment of the central metal atom (local pseudo D_{5h} symmetry) which promotes high anisotropy of the complexes and thereby increases the magnetization barrier [18,33–35]. The PBP coordination with the H₂dapsc ligand has been realized in three 3d-3d cyano-bridged chain compounds with SCM properties. Two of them were synthesized using the strategy to combine $M^{II}(H_2dapsc)$ transition metal complexes with $[M^{III}(CN)_6]^{3-}$ transition metal anions: $\{[Mn(H_2dapsc)][Mn(CN)_6][K(H_2O)_{2.75}(MeOH)_{0.5}]\}_n \cdot 0.5nH_2O$ and $\{[Mn(H_2dapsc)][Fe(CN)_6][K(H_2O)_{3.5}]\}_n \cdot 1.5nH_2O$ [36,37]. The third compound $[Cr(dapbh)(CN)_2Fe(H_2dapsc)]PF_6$ is the product of a reaction between two pentagonal-bipyramidal units: $[Fe(H_2dapsc)Cl_2]$ and $[Cr(dapbh)(CN)_2]^-$ [38]. In all three structures, the M^{II} center is seven-coordinated by N₃O₂ atoms of the H₂dapsc ligand in the equatorial plane and two axial N atoms from the two CN-linkers. Owing to PBP geometry, these SCM complexes have approximately linear structure of the chains in which $M^{II}(H_2dapsc)$ units are connected through a pair of CN-groups in *trans*-geometry with respect to metal ions and H₂dapsc moieties are near orthogonal to the chain direction. However, heavy lanthanide ions show tendency to the higher degree of coordination. Indeed, in the known Tb, Dy, Er mononuclear complexes with similar N₃O₂ ligands Ln^{3+} ion is mainly eight-, nine- or ten-coordinated whereas seven-coordinated complexes are rarely obtained [39–43]. Linear cyano-bridged chains for Ln complexes with the N₃O₂ pentadentate ligands are not known although for some Ln complexes with other ligands approximately linear chains exist in spite of eight- or nine-coordinated Ln [31,44–49]. To the best of our knowledge the linear chains with seven-coordinate lanthanides have been synthesized only in the case of Dy and Er complexes with the 2-picoline N-oxide ligand in the equatorial plane (five ligand molecules) and two $[M(CN)_6]^{3-}$ anions in the apical positions [50].

In our syntheses the initial Ln complexes were nine-coordinated and we did not obtain linear chain. In any case, the compounds **1–4** are the first examples of the 1D cyano-bridged chain Ln complexes with pentadentate (N₃O₂) ligand. To date, the sole examples of cyano-bridged Ln-based compounds with H₂dapsc analogue (H₂L^{N₃O₂}) are tetranuclear ensembles $\{[Ln(H_2L^{N_3O_2})(H_2O)(DMF)]M(CN)_6\}_2$ ($Ln = Tb, Dy, Ho; M = Co, Fe$) [51], which contain very similar to **1–4** structural motifs of alternated nine-coordinated Ln centers and octahedral anions locked into square instead of infinite chain. Interestingly, that SMM properties are found for the Dy complex with diamagnetic Co³⁺ cation whereas Dy complex with paramagnetic Fe³⁺ does not show a slow magnetic relaxation.

2.3. Magnetic Properties

The temperature dependence of the magnetic susceptibility was measured on polycrystalline samples of complexes **1–4** in the temperature range of 2.0–300 K under the applied magnetic field of 0.1 T. The $\chi_{\text{mol}}T$ vs. T plots are depicted in Figure 4. At 300 K, the $\chi_{\text{mol}}T$ values for the complexes are 16.045, 14.545, 15.945 and 14.445 $\text{cm}^3\text{K mol}^{-1}$ and are close to the expected those of 15.94, 14.44, 16.04 and 14.54 $\text{cm}^3\text{K mol}^{-1}$ for **1**, **2**, **3** and **4**, respectively, as the sum of one non-interacting $\text{Dy}^{\text{III}}/\text{Ho}^{\text{III}}$ ion ($14.17 \text{ cm}^3\text{K mol}^{-1}$ for Dy and $14.07 \text{ cm}^3\text{K mol}^{-1}$ for Ho) and one free $\text{Cr}^{\text{III}}/[\text{Fe}^{\text{III}}]_{\text{LS}}$ ($1.87 \text{ cm}^3\text{K mol}^{-1}$ for Cr and $0.37 \text{ cm}^3\text{K mol}^{-1}$ for Fe) [52].

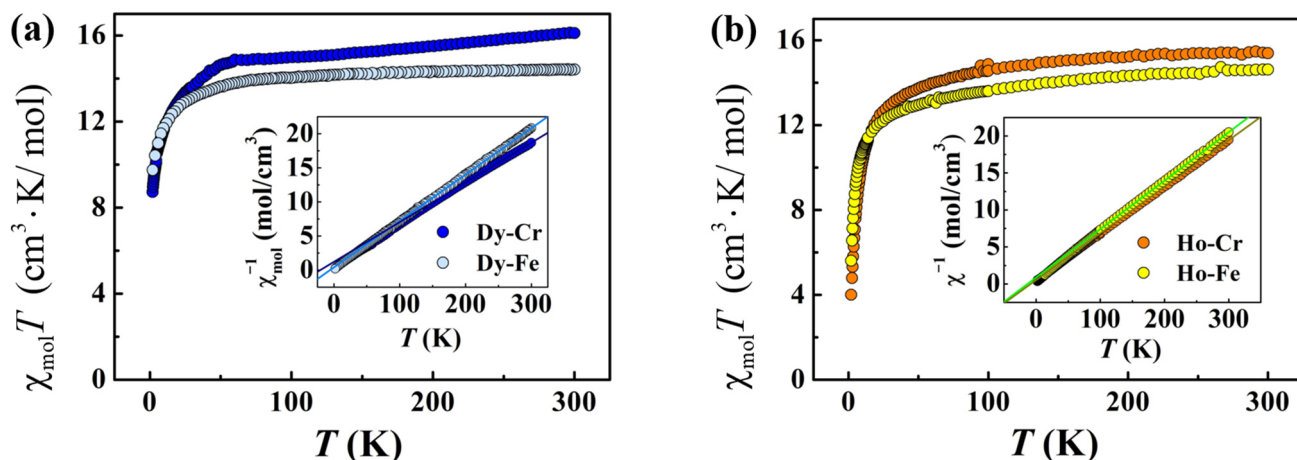


Figure 4. Temperature dependences of the χT product for the complexes **1**_{DyCr}, **2**_{DyFe} (a) and **3**_{HoCr}, **4**_{HoFe} (b). The insets show the temperature dependences of inversed value of magnetic susceptibility with the linear approximations within 150–300 K temperature ranges, extrapolated to full scale of the temperature axis.

On cooling, $\chi_{\text{mol}}T$ values decrease slowly and then their fall accelerates rapidly below 50 K, which may be mainly attributed to the progressive depopulation of the Dy^{III} or Ho^{III} Stark sublevels [6] and magnetic interactions between the 3d and rare-earth ions. The magnetic susceptibility data in the high temperature region (150–300 K) for all complexes obey the Curie-Weiss law with the Weiss constants (θ) being -21.0 , -5.8 , -8.4 and -13.5 K for **1**, **2**, **3**, and **4**, respectively. The nature of the $\text{Dy}^{\text{III}}/\text{Ho}^{\text{III}}\text{-Cr}^{\text{III}}/\text{Fe}^{\text{III}}$ magnetic coupling in complexes **1–4** is usually difficult to assess because of the significant spin-orbit interaction of $\text{Dy}^{\text{III}}/\text{Ho}^{\text{III}}$ ions. Comparative study of the magnetic properties of two tetranuclear quadrangle complexes $[\text{Dy}(\text{H}_2\text{L}^{\text{N}3\text{O}2})(\text{H}_2\text{O})(\text{DMF})\text{M}(\text{CN})_6]_2$ and two binuclear linear Dy-NC-M complexes with the hexacyanides of paramagnetic and diamagnetic 3d-metal ($\text{M} = \text{Fe, Co}$), each of which is linked through a pair of *cis*-cyano groups to two Dy or one cyano group to one Dy, respectively, showed that the interaction between Dy and Fe takes place and is antiferromagnetic [51,53].

In order to examine possible SMM properties of the complexes **1–4**, the ac susceptibility was studied at zero dc field with $H_{\text{ac}} = 4$ Oe. The ac measurements serve as a probe for the relaxation processes in the magnetic system, revealing in a frequency dependence of in-phase $\chi'(f)$ and a non-zero out-of-phase $\chi''(f)$ signal. None of these compounds shows the slow magnetic relaxation in a zero dc magnetic fields; the χ'' signals are not observed, Figure S1.

It is well known that magnetic relaxation of SMMs based on 4f elements is highly susceptible to quantum tunneling of magnetization (QTM), which can be suppressed by applying an external dc field [2,54]. The dc field-dependencies of ac susceptibility (χ' and χ'') were recorded under fields of 0–10000 Oe in search for an optimal field to suppress the QTM effect, Figure 5. When applying a dc field of 1000–2000 Oe, a maximum of χ'' was observed in the case of DyCr (**1**) and DyFe (**2**) complexes.

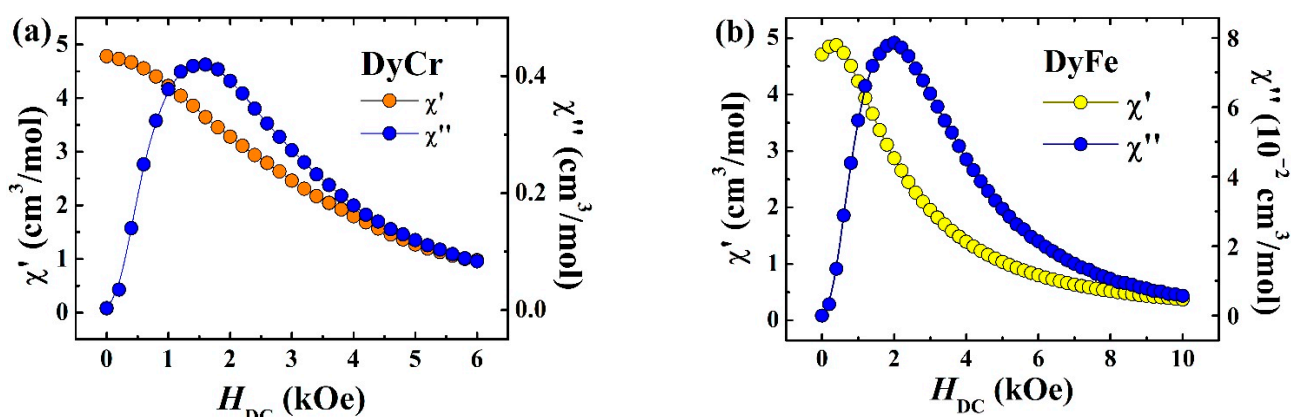


Figure 5. Effect of dc field on the real and imaginary parts of the low-temperature ac magnetic susceptibility of the complexes **1**, (a) DyCr and **2**, (b) DyFe. The curves were recorded at $T = 1.8\text{ K}$, $f = 100\text{ Hz}$ and $h_{\text{ac}} = 4\text{ Oe}$ for the sample **1** and $T = 2.0\text{ K}$, $f = 117\text{ Hz}$ and $h_{\text{ac}} = 5\text{ Oe}$ for the sample **2**.

In contrast to the Dy Kramers ion, the complexes of non-Kramers Ho ion (**3**, **4**) did not show a maximum of χ'' in dc fields up to 6000 Oe, that is, they are not field-induced SMMs. The SMM-silence was also observed for the tetranuclear complex of another non-Kramers ion (Tb), $[\text{Tb}(\text{H}_2\text{L}^{\text{N}3\text{O}2})(\text{H}_2\text{O})(\text{DMF})\text{Co}(\text{CN})_6]_2$, in contrast to the analogous complex of Dy [51]. The crystal-field analysis of the initial mononuclear $[\text{Ln}(\text{H}_2\text{dapsc})(\text{H}_2\text{O})_4](\text{NO}_3)_3$ complexes showed that in the case of non-Kramers Tb and Ho ions, their ground state in these complexes is a well-isolated non-magnetic singlet, which explains the absence of SCM behavior of the nine-coordination Tb and Ho complexes [19]. The deeper drop of the χT product at low temperatures, observed in Ho complexes (**3**, **4**) as compared with Dy complexes (**1**, **2**), Figure 4, reflects this feature of the Ho complexes electronic structure [19,55].

To probe the relaxation behavior of **1** (DyCr) and **2** (DyFe) complexes, the ac susceptibility was studied in a dc field of 1000 Oe at different frequencies (Figure 6). Both the in-phase χ' and out-of-phase χ'' susceptibilities show frequency dependent signals in the temperature range of 1.8 to 2.6 K indicating slow relaxation of magnetization. However, at temperatures above 2.6 K, the χ'' maxima lie above 1400 and 10,000 Hz for **1** and **2**, respectively (maximum frequencies available to us). Assuming that the relaxation of magnetization in **1** and **2** is Debye process driven by the thermal activation over the energy barrier U_{eff} we estimated the values of energy barrier U_{eff} and τ_0 using the Formula (1), proposed in [56].

$$\ln(\chi''/\chi') = \ln(\omega\tau_0) + \frac{U_{\text{eff}}}{kT} \quad (1)$$

where ω ($\omega = 2\pi f$)—is angular frequency, τ_0 is a preexponential factor of the Arrhenius law $\tau = \tau_0 \exp(U_{\text{eff}}/kT)$, T —absolute temperature, U_{eff} —the effective energy barrier for the reversal of magnetization, k —Boltzmann constant.

The experimental plots $\ln(\chi''/\chi')$ vs. T^{-1} at different frequencies and their fitting by the Formula (1) are presented in Figure 7. The average values of U_{eff} and τ_0 are 3.8 K and $1.3 \times 10^{-5}\text{ s}$ and 3.3 K and $1.0 \times 10^{-6}\text{ s}$ for **1** and **2**, respectively. The τ_0 lies in the range values, which are comparable to those of SIMs based on ions of transition metals (τ_0 in the range of $\sim 10^{-5}\text{--}10^{-11}\text{ s}$ [57]). The energy barriers of magnetization for the complexes **1** and **2** are practically the same that is probably a consequence of the same ligand environment of Dy in these compounds, which plays a critical role, since it can affect the local magnetic anisotropy of the rare earth element [6]. Let us consider the possible reasons of the low values of the energy barriers of magnetization for the complexes **1** and **2**, in particular, in comparison with the initial mononuclear complex $[\text{Dy}(\text{H}_2\text{dapsc})(\text{H}_2\text{O})_4]^{3+}$ (3.8 K vs. 18 K). During the synthesis of **1** and **2**, two weak neutral donor ligands (water molecules) of the initial complex are replaced by negatively charged hexacyanometallate building blocks. The *cis*-cyano attachment of these blocks leads to the formation of square-wave

cyano-bridged chains, in which the angles between CN-Ln-NC and M-Ln-M are 73–75° and 101°, respectively. Two $[M(CN)_6]^{3-}$ moieties are attached to Ln^{3+} ion on the same side of H_2dapsc ligand increasing its non-planarity (Figure 2, right). The dihedral angle between two semi-carbazone halves of H_2dapsc is 21.52 and 22.73° in **1** and **2**, respectively, while this angle in the initial mononuclear complex is about 13° [19]. The introduction of negatively charged groups (CN) into the coordination center and the nonlinear nature of one-dimensional M-CN-Ln-NC-M chains lead to strong electrostatic repulsion between the ligands and 4f electron density of the Dy ion and, as a result, to a destabilization of the Dy^{III} oblate nature and weakening the SMM behavior. In addition, the weak antiferromagnetic coupling in **1** and **2** between Dy^{III} and M^{III} ($M = Cr, Fe$) ions through a cyano bridge has a negative effect on the manifestation of the SMM behavior, leading to enhancing the QTM and reducing the energy barrier, as shown in the works [23,28,51,53].

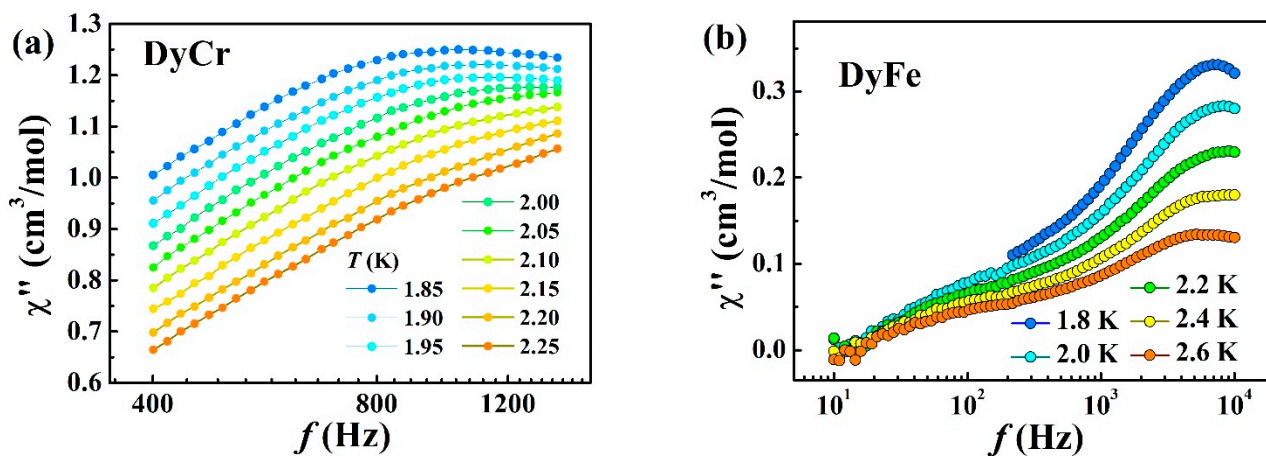


Figure 6. Imaginary parts of ac magnetic susceptibility for the **1** (DyCr) (a) and **2** (DyFe) (b) complexes, measured at the externally applied magnetic field $H_{dc} = 1$ kOe.

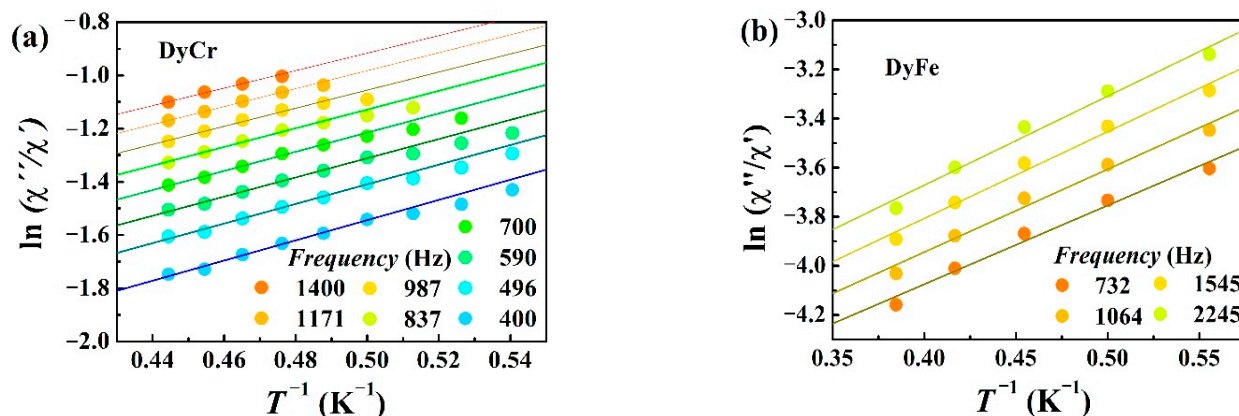


Figure 7. $\ln(\chi''/\chi')$ vs. $1/T$ plots for **1** (a) and **2** (b) at different frequencies of ac field. The solid color lines are the approximations by Equation (1) (see text).

3. Materials and Methods

3.1. Synthesis

All chemicals were used as received from Aldrich without further purification.

The ligand H_2dapsc was prepared following the method described in [58].

The starting compounds $[Dy(H_2dapsc)(H_2O)_4](NO_3)_3$ and $[Ho(H_2dapsc)(H_2O)_4](NO_3)_3$ were synthesized according to the procedure reported previously [19]. The C, H and N elemental analyses were carried out with a Vario Micro Cube analyzing device. The Raman and IR spectra were measured on solid samples using a VERTEX 70v (Bruker) spectrometer on the range of $4000\text{--}500\text{ cm}^{-1}$.

- $\{[\text{Dy}(\text{H}_2\text{dapsc})(\text{H}_2\text{O})_2][\text{Cr}(\text{CN})_6]\}_n \cdot 3n\text{H}_2\text{O}$ (**1**)

The crystals of **1** were obtained by slow diffusion of 3 mL water solution of $\text{K}_3\text{Cr}(\text{CN})_6$ (13.5 mg, 0.041 mmol) through frit with a pore diameter of 10–20 microns into a water solution of $[\text{Dy}(\text{H}_2\text{dapsc})(\text{H}_2\text{O})_4](\text{NO}_3)_3$ (29 mg, 0.041 mmol) in 5 mL H_2O for 7 days at room temperature. The resulting crystals were filtered, washed with H_2O and dried in vacuum. Yield: 22 mg (73%). Anal. calcd. (%) for $\text{C}_{17}\text{H}_{25}\text{N}_{13}\text{O}_7\text{CrDy}$: C, 27.67; H, 3.41; N, 24.67. Found (%): C, 27.96; H, 3.49; N, 24.52. Characteristic Raman data (cm^{-1}): $\nu(\text{C}\equiv\text{N})$ 2150, 2135; $\nu(\text{C}=\text{N})$ 1632 (imine). The bands of stretching vibrations of H_2O and NH do not appear in the Raman spectra, since they have a very low intensity. In the IR spectra, the bands of stretching vibrations of H_2O and NH group are observed in the region of 3180–3400 cm^{-1} (Figures S3, S5 and S8) [59,60].

- $\{[\text{Dy}(\text{H}_2\text{dapsc})(\text{H}_2\text{O})_2][\text{Fe}(\text{CN})_6]\}_n \cdot 3n\text{H}_2\text{O}$ (**2**)

The crystals of **2** were also obtained by slow diffusion but with replacement of $\text{K}_3\text{Cr}(\text{CN})_6$ by $\text{K}_3\text{Fe}(\text{CN})_6$. Yield: 60%. Anal. calcd. (%) for $\text{C}_{17}\text{H}_{25}\text{N}_{13}\text{O}_7\text{FeDy}$: C, 27.52; H, 3.40; N, 24.55. Found (%): C, 27.52; H, 3.57; N, 24.28. Characteristic Raman data (cm^{-1}): $\nu(\text{C}\equiv\text{N})$ 2130, 2119; $\nu(\text{C}=\text{N})$ 1627 (imine) (Figure S2).

- $\{[\text{Ho}(\text{H}_2\text{dapsc})(\text{H}_2\text{O})_2][\text{Cr}(\text{CN})_6]\}_n \cdot 3n\text{H}_2\text{O}$ (**3**)

The water solution (3 mL) of $\text{K}_3\text{Cr}(\text{CN})_6$ (20 mg, 0.062 mmol) and the solution of $[\text{Ho}(\text{H}_2\text{dapsc})(\text{H}_2\text{O})_4](\text{NO}_3)_3$ (43 mg, 0.062 mmol) in 5 mL H_2O and 1 mL ethanol were added by slow diffusion to 10 mL H_2O . The mixture was left undisturbed at room temperature for 1–2 days. The resulting crystals of **3** were filtered, washed with water and dried in vacuum. Yield: 38 mg (83%). Anal. calcd. (%) for $\text{C}_{17}\text{H}_{25}\text{N}_{13}\text{O}_7\text{CrHo}$: C, 27.58; H, 3.40; N, 24.60. Found (%): C, 27.48; H, 3.50; N, 24.51. Characteristic Raman data (cm^{-1}): $\nu(\text{C}\equiv\text{N})$ 2145, 2132; $\nu(\text{C}=\text{N})$ 1633 (imine) (Figure S4).

The thermogram of the complex **3** (Figure S6) demonstrates a mass loss of 5.51% in the temperature range 50–100 °C with an endothermic peak at 93 °C which corresponds to the loss of lattice H_2O molecules. The second endothermic peak at 157.3 °C with a mass loss of 4.81% corresponds to a loss of coordinated H_2O molecules. In the mass spectrum recorded in the gas phase the peaks are observed at $m/z = 18$ and $m/z = 17$ from H_2O molecules. The decomposition of the complex starts above 200 °C and is accompanied by the release of CN^- ($m/z = 26$), OH^- ($m/z = 18, 17$) and CH_3^- ($m/z = 15$) fragments.

- $\{[\text{Ho}(\text{H}_2\text{dapsc})(\text{H}_2\text{O})_2][\text{Fe}(\text{CN})_6]\}_n \cdot 3n\text{H}_2\text{O}$ (**4**)

The crystals of **4** were obtained by the same method of the preparation for **3** but with using of $\text{K}_3\text{Fe}(\text{CN})_6$. Yield: 63%. Anal. calcd. (%) for $\text{C}_{17}\text{H}_{25}\text{N}_{13}\text{O}_7\text{FeHo}$: C, 27.43; H, 3.38; N, 24.46. Found (%): C, 27.37; H, 3.40; N, 23.98. Characteristic Raman data (cm^{-1}): $\nu(\text{C}\equiv\text{N})$ 2142, 2127; $\nu(\text{C}=\text{N})$ 1627 (imine) (Figure S7).

The thermal analysis of crystals **4** showed a weight loss in the temperature range 40–100 °C and 115–170 °C corresponding to the loss of lattice and coordinated water molecules, respectively (Figure S9). In the mass spectrum of the gas phase the peaks at $m/z = 18$ and 17 from H_2O molecules are observed. The decomposition of complex **4** with the release of CN-fragments begins at 180–200 °C.

3.2. X-ray Crystal Structure

X-ray single crystal diffraction data were collected at different temperatures on an Oxford Diffraction Gemini-R CCD diffractometer equipped with an Oxford cryostream cooler [$\lambda(\text{MoK}_\alpha) = 0.71073 \text{ \AA}$, graphite monochromator, ω -scans]. Single crystals were taken from the mother liquid using a nylon loop with paratone oil and immediately transferred into cold nitrogen stream of the diffractometer. Data reduction with empirical absorption correction of experimental intensities (Scale3AbsPack program) was made with the CrysAlisPro software [61].

The structures were solved by direct method and refined by a full-matrix least squares method using SHELX-2016 program [62]. Experimental data for **2** were collected from the twinned crystal (twin operation is 180° rotation around the *c*-axis) and HKLF5 instruction

of SHELXL was used for the structure refinement. All non-hydrogen atoms were refined anisotropically. The positions of H-atoms were calculated geometrically and refined in a riding model with isotropic displacement parameters depending on U_{eq} of connected atom. Torsion angles for $-\text{CH}_3$ hydrogens were refined using HFIX137. The hydrogen atoms of water molecules were found from difference Fourier map and refined isotropically with $U_{\text{iso}}(\text{H}) = 1.5U_{\text{eq}}(\text{O})$ and bond lengths restraints (SADI). Main crystal data, the X-ray data collection and refinement statistics for **1–4** are listed in Table 1. CCDC 2156616–2156619 contain the supplementary crystallographic data for this paper. These data can be obtained free of charge via <http://www.ccdc.cam.ac.uk/conts/retrieving.html> accessed on 10 February 2022 (or from the CCDC, 12 Union Road, Cambridge CB2 1EZ, UK; Fax: +44 1223 336033; E-mail: deposit@ccdc.cam.ac.uk).

3.3. Magnetic Measurements

The dc of powder samples **1–4** was measured by a Quantum Design MPMS-5 SQUID magnetometer. Ac measurements were carried out on a MPMS-5 for complexes **1, 3, 4** and Physical Properties Measurements System PPMS-9 (Quantum Design) for complex **2**. The experimental data were corrected for the sample holder and for the diamagnetic contribution calculated from Pascal constants.

4. Conclusions

Four new cyano-bridged DyCr (**1**), DyFe (**2**), HoCr (**3**) and HoFe (**4**) bimetallic coordination polymers of the $\{[\text{Ln}(\text{H}_2\text{daps})_2(\text{H}_2\text{O})_2][\text{M}(\text{CN})_6]\}_n \cdot 3n\text{H}_2\text{O}$ composition were synthesized by the reaction of $[\text{Ln}^{3+}(\text{H}_2\text{daps})(\text{H}_2\text{O})_4](\text{NO}_3)_3$ ($\text{Ln}^{3+} = \text{Dy, Ho}$) with $\text{K}_3[\text{M}^{3+}(\text{CN})_6]$ ($\text{M}^{3+} = \text{Cr, Fe}$) in water. X-ray single crystal diffraction study showed that the complexes **1–4** are isostructural to each other and have 1D chain structure. The chains are composed by alternating cationic $[\text{Ln}(\text{H}_2\text{daps})(\text{H}_2\text{O})_2]^{3+}$ and anionic $[\text{M}(\text{CN})_6]^{3-}$ units linked by CN-ligands of the anion which are located in the *cis*-position with respect to metal ions. As a result, the chains have square-wave topology which is supported by strong hydrogen bonding. The Ln^{3+} ion is nine-coordinated by N_3O_2 atoms of the H_2daps ligand, two N of CN-bridges and two O of coordinated H_2O molecules.

The compounds **1–4** are the first examples of the 1D cyano-bridged chain Ln complexes with pentadentate (N_3O_2) ligand. The dc magnetic measurements indicated possible antiferromagnetic coupling between the 3d and 4f metal ions. The 300 K $\chi_{\text{mol}}T$ values correspond to the practically non-interacting Ln^{3+} and M^{3+} magnetic centers. According to the ac measurements, the DyCr (**1**) and DyFe (**2**) complexes containing Dy^{3+} Kramers ion behave as field-induced single molecule magnets, while their non-Kramers Ho analogs do not exhibit slow magnetic relaxation. The lower values of the magnetization barrier for complexes **1** and **2** compared to the initial mononuclear complex $[\text{Dy}(\text{H}_2\text{daps})(\text{H}_2\text{O})_4](\text{NO}_3)_3$ are observed. The introduction of negatively charged groups (CN) into the coordination center and the nonlinear nature of one-dimensional M-CN-Ln-NC-M chains lead to strong electrostatic repulsion between the ligands and 4f electron density of the Dy ion and, as a result, to a destabilization of the Dy^{III} oblate nature and weakening the SMM behavior.

Supplementary Materials: The following supporting information can be downloaded at: <https://www.mdpi.com/article/10.3390/inorganics10040041/s1>, Cif and CheckCif files; Figure S1: Real and imaginary parts of ac magnetic susceptibility for the **1** (DyCr) and **2** (DyFe) complexes, measured without an externally applied magnetic field; Figure S2: Raman spectrum of the complex **2** (DyFe); Figure S3: IR spectrum of the complex **2** (DyFe); Figure S4: Raman spectrum of the complex **3** (HoCr); Figure S5: IR spectrum of the complex **3** (HoCr); Figure S6: TG-DSC curves and mass spectra for complex **3** (HoCr) after drying in vacuum; Figure S7: Raman spectrum of the complex **4** (HoFe); Figure S8: IR spectrum of the complex **4** (HoFe); Figure S9: TG-DSC curves and mass spectra for complex **4** (HoFe) after drying in vacuum; Table S1: SHAPE analysis; Table S2: Hydrogen bond geometry in DyCr complex **1**; Table S3: Hydrogen bond geometry in DyFe complex **2**; Table S4: Hydrogen bond geometry in HoCr complex **3**; Table S5: Hydrogen bond geometry in HoFe complex **4**.

Author Contributions: V.D.S.—synthesis of the compounds; S.V.S.—single-crystal X-ray diffraction study; A.D.T.—magnetic measurements, formal analysis; L.V.Z.—writing, original draft preparation; E.B.Y.—data curation, writing, review and editing. All authors have read and agreed to the published version of the manuscript.

Funding: This research was funded by the Ministry of Science and Higher Education within the State assignment for IPCP RAS, state registration number: AAAA-A19-119092390079-8 and AAAA-A19-119061890019-5. The structural study was supported by the Ministry of Science and Higher Education within the State assignment for ISSP RAS.

Data Availability Statement: Not applicable.

Acknowledgments: This work was performed using the equipment of the Research Centre, IPCP RAS, <https://icp.ac.ru/en/>.

Conflicts of Interest: The authors declare no conflict of interest.

Appendix A

Table A1. Selected bond lengths (\AA) and angles ($^\circ$) in 1–4.

	1 (DyCr)	2 (DyFe)	3 (HoCr)	4 (HoFe)
Ln(1)-O(1)	2.3279(9)	2.317(5)	2.326(1)	2.321(4)
Ln(1)-O(2)	2.3627(9)	2.354(4)	2.357(1)	2.363(4)
Ln(1)-N(5)	2.5272(11)	2.525(5)	2.522(1)	2.535(5)
Ln(1)-N(6)	2.5654(11)	2.560(5)	2.564(1)	2.551(4)
Ln(1)-N(7)	2.5152(12)	2.499(5)	2.510(2)	2.496(5)
Ln(1)-N(12)	2.5288(12)	2.536(5)	2.521(2)	2.547(4)
Ln(1)-N(13)	2.5080(12)	2.516(5)	2.502(2)	2.521(5)
Ln(1)-O(3)	2.3508(10)	2.359(4)	2.347(1)	2.373(4)
Ln(1)-O(4)	2.3589(10)	2.349(5)	2.355(1)	2.362(4)
M(1)-C _{CN}	2.0575(14)–2.0798(13)	1.925(7)–1.968(7)	2.063(2)–2.088(2)	1.918(6)–1.968(5)
Ln(1)-M(1)	5.6295(2)	5.5190(12)	5.6355(4)	5.5525(9)
Ln(1)-M(1) *	5.5982(2)	5.4749(12)	5.5999(4)	5.4918(12)
O(1)-Ln(1)-O(2)	97.74(3)	96.12(16)	97.23(5)	95.68(13)
O(1)-Ln(1)-N(5)	64.07(4)	64.17(17)	64.13(5)	64.42(14)
O(2)-Ln(1)-N(6)	63.34(3)	63.73(16)	63.44(5)	63.88(14)
N(5)-Ln(1)-N(7)	61.75(4)	61.97(19)	62.11(5)	62.08(14)
N(6)-Ln(1)-N(7)	61.46(4)	61.72(18)	61.50(5)	61.45(14)
O(1)-Ln(1)-N(6)	147.76(4)	146.47(17)	147.49(5)	145.52(14)
O(2)-Ln(1)-N(5)	147.23(3)	146.28(16)	147.01(5)	146.58(13)
O(3)-Ln(1)-O(4)	129.47(4)	129.84(19)	129.37(5)	129.8(2)
N(12)-Ln(1)-N(13)	73.08(4)	74.94(16)	73.18(5)	74.76(14)
Ln(1)-N(12)-C(12)	158.95(10)	160.2(5)	159.15(15)	159.4(4)
Ln(1)-N(13)-C(13)	155.25(10)	154.9(5)	155.45(15)	154.5(4)
M(1)-C(12)-N(12)	174.59(11)	175.1(6)	174.5(2)	176.0(5)
M(1)-C(13) **-N(13) **	176.37(13)	177.9(6)	176.3(2)	178.0(5)
C(12)-M(1)-C(13) **	94.26(5)	94.8(3)	94.37(7)	94.9(2)
M(1)-Ln(1)-M(1) *	100.72(0)	101.05(2)	100.77(0)	101.02(1)
Ln(1)-M(1)-Ln(1) **	95.61(0)	95.78(2)	95.67(0)	95.90(1)

Symmetry codes: * (1 – x , 0.5 + y , 0.5 – z), ** (1 – x , y – 0.5, 0.5 – z).

References

- Bartolomé, J.; Luis, F.; Fernández, J.F. *Molecular Magnets: Physics and Applications*; Springer: Berlin/Heidelberg, Germany, 2014.
- Layfield, R.A.; Murugesu, M. *Lanthanides and Actinides in Molecular Magnetism*; Wiley-VCH Verlag & Co. KGaA: Weinheim, Germany, 2015.
- Dey, A.; Kalita, P.; Chandrasekhar, V. Lanthanide(III)-Based Single-Ion Magnets. *ACS Omega* **2018**, *3*, 9462–9475. [CrossRef] [PubMed]
- Bar, A.K.; Pichon, C.; Sutter, J.-P. Magnetic anisotropy in two- to eight-coordinated transition–metal complexes: Recent developments in molecular magnetism. *Co-Ord. Chem. Rev.* **2016**, *308*, 346–380. [CrossRef]

5. Meng, Y.-S.; Jiang, S.-D.; Wang, B.-W.; Gao, S. Understanding the Magnetic Anisotropy toward Single-Ion Magnets. *Acc. Chem. Res.* **2016**, *49*, 2381–2389. [CrossRef] [PubMed]
6. Rinehart, J.D.; Long, J.R. Exploiting single-ion anisotropy in the design of f-element single-molecule magnets. *Chem. Sci.* **2011**, *2*, 2078–2085. [CrossRef]
7. Feng, M.; Tong, M.-L. Single ion magnets from 3d to 5f: Developments and strategies. *Chem. Eur. J.* **2018**, *24*, 7574–7594. [CrossRef] [PubMed]
8. Chen, Y.-C.; Liu, J.-L.; Ungur, L.; Liu, J.; Li, Q.-W.; Wang, L.-F.; Ni, Z.-P.; Chibotaru, L.F.; Chen, X.-M.; Tong, M.-L. Symmetry-Supported Magnetic Blocking at 20 K in Pentagonal Bipyramidal Dy(III) Single-Ion Magnets. *J. Am. Chem. Soc.* **2016**, *138*, 2829–2837. [CrossRef] [PubMed]
9. Liu, J.; Chen, Y.-C.; Liu, J.-L.; Vieru, V.; Ungur, L.; Jia, J.-H.; Chibotaru, L.F.; Lan, Y.; Wernsdorfer, W.; Gao, S.; et al. A Stable Pentagonal Bipyramidal Dy(III) Single-Ion Magnet with a Record Magnetization Reversal Barrier over 1000 K. *J. Am. Chem. Soc.* **2016**, *138*, 5441–5450. [CrossRef] [PubMed]
10. Ding, Y.; Chilton, N.F.; Winpenny, R.E.P.; Zheng, Y.-Z. On Approaching the Limit of Molecular Magnetic Anisotropy: A Near-Perfect Pentagonal Bipyramidal Dysprosium(III) Single-Molecule Magnet. *Angew. Chem. Int. Ed.* **2016**, *55*, 16071–16074. [CrossRef] [PubMed]
11. Gupta, S.K.; Rajeshkumar, T.; Rajaraman, G.; Murugavel, R. An air-stable Dy(iii) single-ion magnet with high anisotropy barrier and blocking temperature. *Chem. Sci.* **2016**, *7*, 5181–5191. [CrossRef]
12. Yu, K.-X.; Kragskow, J.; Ding, Y.; Zhai, Y.-Q.; Reta, D.; Chilton, N.F.; Zheng, Y.-Z. Enhancing Magnetic Hysteresis in Single-Molecule Magnets by Ligand Functionalization. *Chem* **2020**, *6*, 1777–1793. [CrossRef]
13. Palenik, G.J.; Wester, D.W. Pentagonal-bipyramidal complexes. Crystal and molecular structures of chloroaqua(2,6-diacetylpyridine bis(semicarbazone))manganese(II), -iron(II), -cobalt(II), and -zinc(II) chloride dihydrates. *Inorg. Chem.* **1978**, *17*, 864–870. [CrossRef]
14. Gerloch, M.; Morgenstern-Badarau, I. Magnetic and spectral properties of chloroaqua[2,6-diacetylpyridinebis(semicarbazone)]iron(II) and diaqua[2,6-diacetylpyridinebis(semicarbazone)]nickel(II): Ligand fields and bonding in pentagonal-bipyramidal complexes. *Inorg. Chem.* **1979**, *18*, 3225–3229. [CrossRef]
15. Ivanovic-Burmazovic, I.; Andjelkovic, K. Transition Metal Complexes with Bis(hydrazone) Ligands of 2,6-Diacetylpyridine: Heptacoordination of 3d Metals. *Adv. Inorg. Chem.* **2005**, *36*, 315–360. [CrossRef]
16. Bino, A.; Frim, R.; Van Genderen, M. Three coordination modes of the pentadentate ligand 2,6-diacetylpyridinedisemicarbazone. *Inorg. Chim. Acta* **1987**, *127*, 95–101. [CrossRef]
17. Carcelli, M.; Ianelli, S.; Pelagatti, P.; Pelizzi, G. Structural characterization of a new ligand mode of 2,6-diacetylpyridine bis(semicarbazone), H₂daps. *Inorg. Chim. Acta* **1999**, *292*, 121–126. [CrossRef]
18. Bar, A.K.; Gogoi, N.; Pichon, C.; Goli, V.M.L.D.P.; Thiljeni, M.; Duhayon, C.; Suaud, N.; Guihéry, N.; Barra, A.-L.; Ramasesha, S.; et al. Pentagonal Bipyramid Fe^{II} Complexes: Robust Ising-Spin Units towards Heteropolynuclear Nanomagnets. *Chem.—Eur. J.* **2017**, *23*, 4380–4396. [CrossRef] [PubMed]
19. Sasnovskaya, V.D.; Kopotkov, V.A.; Kazakova, A.V.; Talantsev, A.D.; Morgunov, R.B.; Simonov, S.V.; Zorina, L.V.; Mironov, V.S.; Yagubskii, E.B. Slow magnetic relaxation in mononuclear complexes of Tb, Dy, Ho and Er with the pentadentate (N₃O₂) Schiff-base dapsc ligand. *New J. Chem.* **2018**, *42*, 14883–14893. [CrossRef]
20. Han, T.; Leng, J.-D.; Ding, Y.-S.; Wang, Y.; Zheng, Z.; Zheng, Y.-Z. Field and dilution effects on the magnetic relaxation behaviours of a 1D dysprosium(III)-carboxylate chain built from chiral ligands. *Dalton Trans.* **2015**, *44*, 13480–13484. [CrossRef]
21. Chen, S.; Mereacre, V.; Zhao, Z.; Zhang, W.; Zhang, M.; He, Z. Targeted replacement: Systematic studies of dodecanuclear {M^{III}₆Ln^{III}₆} coordination clusters (M = Cr, Co; Ln = Dy, Y). *Dalton Trans.* **2018**, *47*, 7456–7462. [CrossRef]
22. Shen, F.-X.; Li, H.-Q.; Miao, H.; Shao, D.; Wei, X.-Q.; Shi, L.; Zhang, Y.-Q.; Wang, X.-Y. Heterometallic M^{II}Ln^{III} (M = Co/Zn; Ln = Dy/Y) Complexes with Pentagonal Bipyramidal 3d Centers: Syntheses, Structures, and Magnetic Properties. *Inorg. Chem.* **2018**, *57*, 15526–15536. [CrossRef]
23. Chen, S.; Mereacre, V.; Kostakis, G.E.; Anson, C.E.; Powell, A.K. Systematic studies of hexanuclear {M^{III}₄Ln^{III}₂} complexes (M = Fe, Ga; Ln = Er, Ho): Structures, magnetic properties and SMM behavior. *Inorg. Chem. Front.* **2017**, *4*, 927–934. [CrossRef]
24. Blagg, R.; Ungur, L.; Tuna, F.; Speak, J.; Comar, P.; Collison, D.; Wernsdorfer, W.; McInnes, E.J.L.; Chibotaru, L.; Winpenny, R.E.P. Magnetic relaxation pathways in lanthanide single-molecule magnets. *Nat. Chem.* **2013**, *5*, 673–678. [CrossRef] [PubMed]
25. Habib, F.; Lin, P.-H.; Long, J.; Korobkov, I.; Wernsdorfer, W.; Murugesu, M. The Use of Magnetic Dilution to Elucidate the Slow Magnetic Relaxation Effects of a Dy₂ Single-Molecule Magnet. *J. Am. Chem. Soc.* **2011**, *133*, 8830–8833. [CrossRef] [PubMed]
26. Rinehart, J.; Fang, M.; Evans, W.J.; Long, J.R. Strong exchange and magnetic blocking in N₂³⁻-radical-bridged lanthanide complexes. *Nat. Chem.* **2011**, *3*, 538–542. [CrossRef]
27. Wang, J.-H.; Li, Z.-Y.; Yamashita, M.; Bu, X.-H. Recent progress on cyano-bridged transition-metal-based single-molecule magnets and single-chain magnets. *Co-Ord. Chem. Rev.* **2021**, *428*, 213617. [CrossRef]
28. Liu, Y.; Chen, Y.-C.; Liu, J.; Chen, W.-B.; Huang, G.-Z.; Wu, S.-G.; Wang, J.; Liu, J.-L.; Tong, M.-L. Cyanometallate-Bridged Didysprosium Single-Molecule Magnets Constructed with Single-Ion Magnet Building Block. *Inorg. Chem.* **2020**, *59*, 687–694. [CrossRef]
29. Kou, H.-Z.; Gao, S.; Jin, X. Synthesis, Crystal Structure, and Magnetic Properties of Two Cyano-Bridged Bimetallic 4f–3d Arrays with One-Dimensional Chain and Two-Dimensional Brick Wall Molecular Structures. *Inorg. Chem.* **2001**, *40*, 6295–6300. [CrossRef]

30. Ge, C.; Kou, H.-Z.; Ni, Z.-H.; Jiang, Y.-B.; Zhang, L.-F.; Cui, A.-L.; Sato, O. Cyano-bridged One-dimensional Sm^{III}–Fe^{III} Molecule-based Magnet with an Ordering Temperature of 3.4 K. *Chem. Lett.* **2005**, *34*, 1280–1281. [CrossRef]
31. Figuerola, A.; Diaz, C.; El Fallah, M.S.; Ribas, J.; Maestro, M.; Mahía, J. Structure and magnetism of the first cyano-bridged hetero-one-dimensional Gd^{III}–Cr^{III} complexes. *Chem. Commun.* **2001**, *1204–1205*. [CrossRef]
32. Guo, Y.; Xu, G.-F.; Wang, C.; Cao, T.-T.; Tang, J.; Liu, Z.-Q.; Ma, Y.; Yan, S.-P.; Cheng, P.; Liao, D.-Z. Cyano-bridged terbium(III)–chromium(III) bimetallic quasi-one-dimensional assembly exhibiting long-range magnetic ordering. *Dalton Trans.* **2012**, *41*, 1624–1629. [CrossRef]
33. Batchelor, L.J.; Sangalli, M.; Guillot, R.; Guihéry, N.; Maurice, R.; Tuna, F.; Mallah, T. Pentanuclear Cyanide-Bridged Complexes Based on Highly Anisotropic Co^{II} Seven-Coordinate Building Blocks: Synthesis, Structure, and Magnetic Behavior. *Inorg. Chem.* **2011**, *50*, 12045–12052. [CrossRef] [PubMed]
34. Ruamps, R.; Batchelor, L.J.; Maurice, R.; Gogoi, N.; Jiménez-Lozano, P.; Guihéry, N.; de Graaf, C.; Barra, A.L.; Sutter, J.-P.; Mallah, T. Origin of the magnetic anisotropy in heptacoordinate Ni^{II} and Co^{II} complexes. *Chem. Eur. J.* **2013**, *19*, 950–956. [CrossRef] [PubMed]
35. Manakin, Y.V.; Mironov, V.S.; Bazhenova, T.A.; Lyssenko, K.A.; Gilmutdinov, I.F.; Bikbaev, K.S.; Masitov, A.A.; Yagubskii, E.B. (Et₄N)[Mo^{III}(DAPBH)Cl₂], the first pentagonal-bipyramidal Mo(III) complex with a N₃O₂-type Schiff-base ligand: Manifestation of unquenched orbital momentum and Ising-type magnetic anisotropy. *Chem. Commun.* **2018**, *54*, 10084–10087. [CrossRef]
36. Sasnovskaya, V.D.; Kopotkov, V.A.; Talantsev, A.D.; Morgunov, R.B.; Yagubskii, E.B.; Simonov, S.V.; Zorina, L.V.; Mironov, V.S. Synthesis, structure and magnetic properties of 1D {[Mn^{III}(CN)₆][Mn^{II}(dapsc)]}_n coordination polymers: Origin of unconventional single-chain magnet behavior. *Inorg. Chem.* **2017**, *56*, 8926–8943. [CrossRef] [PubMed]
37. Zorina, L.V.; Simonov, S.V.; Sasnovskaya, V.D.; Talantsev, A.D.; Morgunov, R.B.; Mironov, V.S.; Yagubskii, E.B. Slow magnetic relaxation, antiferromagnetic ordering and metamagnetism in Mn^{II}(H₂dapsc)-Fe^{III}(CN)₆ chain complex with highly anisotropic Fe-CN-Mn spin coupling. *Chem. Eur. J.* **2019**, *25*, 14583–14597. [CrossRef]
38. Pichon, C.; Suaud, N.; Duhayon, C.; Guihéry, N.; Sutter, J.-P. Cyano-Bridged Fe(II)–Cr(III) Single-Chain Magnet Based on Pentagonal Bipyramid Units: On the Added Value of Aligned Axial Anisotropy. *J. Am. Chem. Soc.* **2018**, *140*, 7698–7704. [CrossRef]
39. Albrecht, M.; Mirtschin, S.; Osetska, O.; Dehn, S.; Enders, D.; Fröhlich, R.; Pape, T.; Hahn, E.F. Pentadentate Ligands for the 1:1 Coordination of Lanthanide(III) Salts. *Eur. J. Inorg. Chem.* **2007**, *2007*, 3276–3287. [CrossRef]
40. Bar, A.K.; Kalita, P.; Sutter, J.-P.; Chandrasekhar, V. Pentagonal-Bipyramidal Ln(III) Complexes Exhibiting Single-Ion-Magnet Behavior: A Rational Synthetic Approach for a Rigid Equatorial Plane. *Inorg. Chem.* **2018**, *57*, 2398–2401. [CrossRef]
41. Corredoira-Vázquez, J.; Fondo, M.; Sanmartin-Matalobos, J.; García-Deibe, A.M. Attainment of pentagonal-bipyramidal Ln^{III} complexes from a planar pentadentate ligand. *Proceedings* **2020**, *62*, 2. [CrossRef]
42. Kalita, P.; Ahmed, N.; Bar, A.K.; Dey, S.; Jana, A.; Rajaraman, G.; Sutter, J.-P.; Chandrasekhar, V. Pentagonal Bipyramidal Ln(III) Complexes Containing an Axial Phosphine Oxide Ligand: Field-induced Single-ion Magnetism Behavior of the Dy(III) Analogue. *Inorg. Chem.* **2020**, *59*, 6603–6612. [CrossRef]
43. Bazhenova, T.A.; Kopotkov, V.A.; Korchagin, D.V.; Manakin, Y.V.; Zorina, L.V.; Simonov, S.V.; Yakushev, I.A.; Mironov, V.S.; Vasiliev, A.N.; Maximova, O.V.; et al. A Series of Novel Pentagonal-Bipyramidal Erbium(III) Complexes with Acyclic Chelating N₃O₂ Schiff-Base Ligands: Synthesis, Structure, and Magnetism. *Molecules* **2021**, *26*, 6908. [CrossRef] [PubMed]
44. Figuerola, A.; Diaz, C.; Ribas, J.; Tangoulis, V.; Sangregorio, C.; Gatteschi, D.; Maestro, M.; Mahía, J. Magnetism of Cyano-Bridged Hetero-One-Dimensional Ln₃₊–M₃₊ Complexes (Ln³⁺ = Sm, Gd, Yb; M³⁺ = Fe_{LS}, Co). *Inorg. Chem.* **2003**, *42*, 5274–5281. [CrossRef] [PubMed]
45. Figuerola, A.; Ribas, J.; Casanova, D.; Maestro, M.; Alvarez, S.; Diaz, C. Magnetism of Cyano-Bridged Ln³⁺–M³⁺ Complexes. Part II: One-Dimensional Complexes (Ln³⁺ = Eu, Tb, Dy, Ho, Er, Tm; M³⁺ = Fe or Co) with bpy as Blocking Ligand. *Inorg. Chem.* **2005**, *44*, 6949–6958. [CrossRef] [PubMed]
46. Koner, R.; Drew, M.G.; Figuerola, A.; Diaz, C.; Mohanta, S. A new cyano-bridged one-dimensional Gd^{III}Fe^{III} coordination polymer with o-phenanthroline as the blocking ligand: Synthesis, structure, and magnetic properties. *Inorg. Chim. Acta* **2005**, *358*, 3041–3047. [CrossRef]
47. Estrader, M.; Ribas, J.; Tangoulis, V.; Solans, X.; Font-Bardía, M.; Maestro, M.; Diaz, C. Synthesis, Crystal Structure, and Magnetic Studies of One-Dimensional Cyano-Bridged Ln³⁺–Cr³⁺ Complexes with bpy as a Blocking Ligand. *Inorg. Chem.* **2006**, *45*, 8239–8250. [CrossRef] [PubMed]
48. Zhao, H.; Lopez, N.; Prosvirin, A.; Chifotides, H.T.; Dunbar, K.R. Lanthanide–3d cyanometalate chains Ln(III)–M(III) (Ln = Pr, Nd, Sm, Eu, Gd, Tb; M = Fe) with the tridentate ligand 2,4,6-tri(2-pyridyl)-1,3,5-triazine (tptz): Evidence of ferromagnetic interactions for the Sm(III)–M(III) compounds (M = Fe, Cr). *Dalton Trans.* **2007**, *878–888*. [CrossRef] [PubMed]
49. Yu, D.; Li, L.; Zhou, H.; Yuan, A.; Li, Y. Cyano-Bridged 4f-3d Assemblies with Achiral Helical Chains: Syntheses, Structures, and Magnetic Properties. *Eur. J. Inorg. Chem.* **2012**, *2012*, 3394–3397. [CrossRef]
50. Wang, F.; Gong, H.-W.; Zhang, Y.; Xue, A.-Q.; Zhu, W.-H.; Zhang, Y.-Q.; Huang, Z.-N.; Sun, H.-L.; Liu, B.; Fang, Y.-Y.; et al. The comparative studies on the magnetic relaxation behaviour of the axially-elongated pentagonal-bipyramidal dysprosium and erbium ions in similar one-dimensional chain structures. *Dalton Trans.* **2021**, *50*, 8736–8745. [CrossRef]
51. Wang, R.; Wang, H.; Wang, J.; Bai, F.; Ma, Y.; Li, L.; Wang, Q.; Zhao, B.; Cheng, P. The different magnetic relaxation behaviors in [Fe(CN)₆]³⁻ or [Co(CN)₆]³⁻ bridged 3d–4f heterometallic compounds. *CrystEngComm* **2020**, *22*, 2998–3004. [CrossRef]

52. Kahn, O. *Molecular Magnetism*; Wiley-VCH: New York, NY, USA, 1993.
53. Zhang, Y.; Guo, Z.; Xie, S.; Li, H.-L.; Zhu, W.-H.; Liu, L.; Dong, X.-Q.; He, W.-X.; Ren, J.-C.; Liu, L.-Z.; et al. Tuning the Origin of Magnetic Relaxation by Substituting the 3d or Rare-Earth Ions into Three Isostructural Cyano-Bridged 3d–4f Heterodinuclear Compounds. *Inorg. Chem.* **2015**, *54*, 10316–10322. [[CrossRef](#)]
54. Thomas, L.; Lointi, F.; Ballou, R.; Gatteschi, D.; Sessoli, R.; Barbara, B. Macroscopic quantum tunnelling of magnetization in a single crystal of nanomagnets. *Nature* **1996**, *383*, 145–147. [[CrossRef](#)]
55. Bazhenova, T.A.; Yakushev, I.A.; Lyssenko, K.A.; Maximova, O.V.; Mironov, V.S.; Manakin, Y.V.; Kornev, A.B.; Vasiliev, A.N.; Yagubskii, E.B. Ten-coordinate lanthanide [Ln(HL)(L)] complexes (Ln = Dy, Ho, Er, Tb) with pentadentate N_3O_2 -type schiff-base ligands: Synthesis, structure and magnetism. *Magnetochemistry* **2020**, *6*, 60. [[CrossRef](#)]
56. Bartolomé, J.; Filoti, G.; Kuncser, V.; Schinteie, G.; Mereacre, V.; Anson, C.E.; Powell, A.K.; Prodius, D.; Turta, C. Magnetostructural correlations in the tetranuclear series of $\{\text{Fe}_3\text{LnO}_2\}$ butterfly core clusters: Magnetic and Mössbauer spectroscopic study. *Phys. Rev. B* **2009**, *80*, 014430. [[CrossRef](#)]
57. Craig, G.A.; Murrie, M. 3d single-ion magnets. *Chem. Soc. Rev.* **2015**, *44*, 2135–2147. [[CrossRef](#)] [[PubMed](#)]
58. Palenik, G.J.; Wester, D.W.; Rychlewska, U.; Palenik, R.C. Pentagonal-bipyramidal complexes. Synthesis and crystal structures of diaqua[2,6-diacetylpyridine bis(semicarbazone)]chromium(III) hydroxide dinitrate hydrate and dichloro[2,6-diacetylpyridine bis(semicarbazone)]iron(III) chloride dehydrate. *Inorg. Chem.* **1976**, *15*, 1814–1819. [[CrossRef](#)]
59. Lorenzini, C.; Pelizzi, C.; Pelizzi, G.; Predieri, G. Investigation into arylhydrazones as chelating agents. Part 3. Synthesis and spectroscopic characterization of complexes of Mn^{II} , Co^{II} , Ni^{II} , Cu^{II} and Zn^{II} with 2,6-diacetylpyridine bis(benzoylhydrazone) and X-ray structure of aquachloro[2,6-diacetylpyridine bis(benzoylhydrazone)]manganese(II) chloride. *J. Chem. Soc. Dalton Trans.* **1983**, 721–727. [[CrossRef](#)]
60. Bonardi, A.; Carini, C.; Merlo, C.; Pelizzi, C.; Pelizzi, G.; Tarasconi, P.; Vitali, F.; Cavatorta, F. Synthesis, spectroscopic and structural characterization of mono- and bi-nuclear iron(II) complexes with 2,6-diacetylpyridine bis(acylhydrazones). *J. Chem. Soc. Dalton Trans.* **1990**, 2771–2777. [[CrossRef](#)]
61. Rigaku Oxford Diffraction Ltd. *CrysAlisPro*; Version 1.171.38; Rigaku Oxford Diffraction Ltd.: Oxford, UK, 2015.
62. Sheldrick, G.M. A short history of SHELX. *Acta Crystallogr. Sect. A* **2008**, *A64*, 112–122. [[CrossRef](#)] [[PubMed](#)]